https://doi.org/10.1016/j.agrformet.2020.108153

Investigating the Urban-induced Microclimate Effects on Winter Wheat Spring Phenology Using Sentinel-2 Time Series

Jiaqi Tian[1], Xiaolin Zhu[1,2]*, Zheyan Shen[1], Jin Wu[3], Shuai Xu[1], Zicong Liang[1], Jingtao Wang[1]

1. Department of Land Surveying and Geo-Informatics, The Hong Kong Polytechnic University, Hong Kong, China

2. Research Institute for Sustainable Urban Development, The Hong Kong Polytechnic University, Hung Hom, Hong Kong, China

3. School of Biological Sciences, Faculty of Science, The University of Hong Kong, Hong Kong, China

*Corresponding author:

Xiaolin Zhu

Address: The Hong Kong Polytechnic University, Room ZS621, Block Z, 181 Chatham Road South, Kowloon, Hong Kong.

Phone: 852-2766-5976; Email: xiaolin.zhu@polyu.edu.hk

Abstract: Temperature is one of the most important factors controlling the phenology of winter wheat. Rapid urbanization in China dramatically modifies the microclimate, especially temperature, surrounding cities. However, it is unclear whether such urban-induced changes in microclimate can influence the phenology of winter wheat and whether the influence is consistent across cities of different sizes. Here, we investigated the urban induced microclimate effects on winter wheat spring phenology (i.e., the regreen-up date, RGUD) in three cities spanning a range of sizes in northern China. These three cities include Shijiazhuang (350.98 km^2), Baoding (118.95 km^2), and Linqing (55.12 km^2), and the key data for this study are Sentinel-2 images. Based on the Sentinel-2 images, we first calculated a vegetation index (normalized difference phenology index, NDPI), and then extracted winter wheat RGUD. Finally, we analyzed the distribution of the RGUD along an urban-rural gradient using buffers surrounding the urban areas. Our study has three main results: (1) The RGUD shows a significant increasing trend along the urban-rural gradients in both Shijiazhuang and Baoding, suggesting that urban-induced increases in temperature indeed advance the spring phenology of winter wheat. (2) The maximum influence size of the urban-induced temperature effects on the RGUD is positively correlated with city size, i.e., 27 km for Shijiazhuang, 14 km for Baoding and 7 km for Linqing. (3) The change rate of the RGUD with distance along the urban-rural gradient is significantly higher in the large city (Shijiazhuang: 0.26 day/km) than it is in the middle- and small-scale cities (Baoding: 0.21 day/km and Linqing: 0.11 day/km), which suggests that larger cities spread heat at a faster rate than that of smaller cities. This study suggests that the planting and management of winter wheat surrounding cities should consider the influence of city size to optimize yields.

Keywords: winter wheat; spring phenology; urban heat island; Sentinel-2 time series; NDPI

1. Introduction

Winter wheat is one of the staple food crops with a large cultivation area on the North China Plain. To ensure efficient crop management and food security, the winter wheat phenological features that generally indicate dates of sowing, emergence, onset of dormancy, regreening (regrowth in spring after dormancy), anthesis, and maturity are collected and supervised by multiple methods (e.g., wheat models, agro-meteorological stations, and satellite-based remotely sensed data) (He et al., 2015; Huang and Lu, 2009; Liu et al., 2018; Xiao et al., 2013). A typical winter wheat growth cycle in northern China corresponding to the vegetation index profile extracted by satellite images is shown in Figure 1. Previous studies have shown that winter wheat spring phenology, i.e., regreen-up date (RGUD), is sensitive to climate and environmental conditions (e.g., temperature, photoperiod and precipitation) (He et al., 2015; Liu et al., 2018; Xiao et al., 2013), and that its shifts can have a substantial influence on energy and carbon exchange, ultimately affecting crop yield and quality (Anwar et al., 2015; Keenan et al., 2014; Tao et al., 2006).

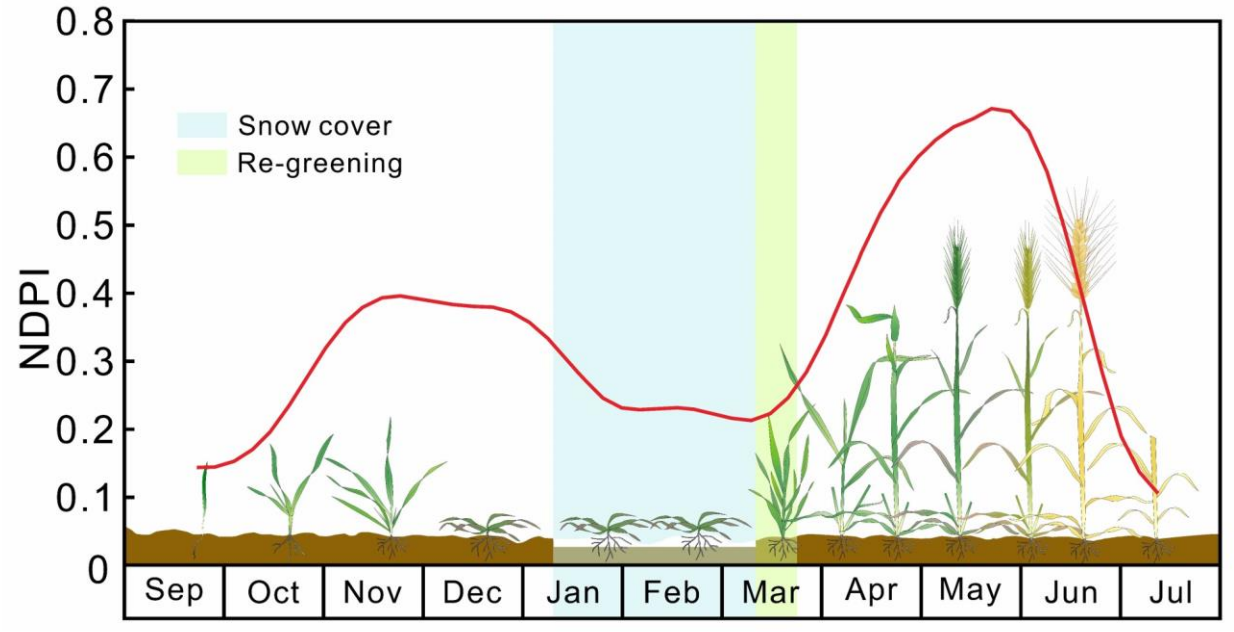

Figure 1. The typical winter wheat growth cycle in northern China corresponding to the NDPI profile extracted by satellite images

Compared with the background of the global climate, urban-induced microclimate changes may be more influential for vegetation growing in urban areas and the surrounding areas (Meng et al., 2020; Wohlfahrt et al., 2010). The urban warming effect is one of the most influential indicators, considering that other environmental factors, for instance, background temperature determined by latitudes, elevations and climate zone, photoperiod and precipitation are very similar within individual cities (Kalnay and Cai, 2003; Sun et al., 2016; Yang et al., 2017). Urban and suburban areas are prone to have higher temperatures than rural areas, a phenomenon referred to as the urban heat island (UHI), mainly induced by the relatively large amount of impervious surfaces as well as the increase in carbon emission into the atmosphere from human activity (Ren et al., 2008). This warming effect is evident from the local to global scale, but the dispersion and gradient of the warming effect can be different across cities with different urban sizes. Given that vegetation growth is highly dependent on geoclimatic factors, it is reasonable

to hypothesize that variability in the increase in temperature along an urban-rural gradient could affect the RGUD of winter wheat and that the strength of this effect may be correlated with urban size.

Previous studies have demonstrated that cropland phenology has been largely affected by the rising temperature, highlighted by the earlier spring phenology and longer growth duration (Cleland et al., 2007; Keenan et al., 2014). The impact of UHIs on the advance of regreening dates shows a decreasing trend with increasing distance from urban areas (Jochner et al., 2012). The urban warming effect largely varies with latitudinal and climatic zone (Lu et al., 2006; Zhou et al., 2016). The species of vegetation is also an influencing factor affecting the phenological response to climate change (Luo et al., 2007). A significant difference in phenological shifts has been found between crops and other natural vegetation, such as grass and mixed forest (Zhang et al., 2004). Additionally, a recent study has also linked the warming effect with urban size, pointing out that a tenfold increase in city size leads to an earlier spring phenology (Li et al., 2016). Although previous studies have investigated the relationship between the urban warming effect and phenological shift, no agreement has been reached due to the inconsistent results from different cities (Lu et al., 2006; Zhang et al., 2004; Zhou et al., 2016). The inconsistency of these results may be attributed to the complex landscape and various vegetation species surrounding urban areas (Chen et al., 2018; Li et al., 2016; Zhang et al., 2017). Using coarse and moderate spatial resolution images, in particular, i.e., the moderate resolution imaging spectroradiometer (MODIS) product, it is difficult to investigate the spatial heterogeneity of winter wheat RGUD along urban-rural gradients. In addition, to explore urban effects on vegetation phenology, previous studies have often focused on cities with similar sizes or individual cities (Qiu et al., 2017; Zhou et al., 2016), so it is not clear whether urban effects on crop phenology differ with urban size.

This study aims to obtain a better understanding of the effects of urban areas on crop phenology. Specifically, the objectives are to examine the spatial heterogeneity of winter wheat RGUD surrounding cities and to investigate whether the spatial pattern is driven by the heat dispersion from the urban heat island or by the microscale sensible heat flux of various land surface materials. Winter wheat was selected to control for the influence of different vegetation species. A dense series of high-resolution satellite images (a total of 23-27 Sentinel-2 images for each city) was used to extract winter wheat cultivation areas as well as phenological feature. A new vegetation index, the normalized difference phenology index (NDPI), which minimizes the effects of snowmelt and soil background, was employed to reflect the good performance of winter wheat growth (Wang et al., 2017). Three cities of different sizes located in the same climatic zone were selected to conduct a comparison of urban effects on winter wheat RGUD while controlling confounding variables such as photoperiod and precipitation.

2. Materials and Methods

2.1. Study Area

Three cities and their surrounding areas in northern China, namely, Shijiazhuang (38° 02' 34"N, 114° 28' 48"E), Baoding (38° 51' 21"N, 115° 28' 48"E) and Linqing (36° 50' 27"N, 115° 43' 12"E), were selected as study areas, as shown in Figure 2. These cities were selected because (1) winter wheat is the main grain crop surrounding them; (2) they are isolated, which reduces interference from other nearby cities; (3) they are on the North China Plain and have similar background climates and low altitudes (<50 m); and (4) they have sufficient clear observations from Sentinel-2 images with which a dense time series can be composed for monitoring the entire growth cycle of winter wheat. Additionally, these cities have different urban population sizes and scales (Figure 2); that is, Shijiazhuang

represents a metropolis, with an urban population of over 5 million people; Baoding represents a medium-sized city (3 million people); and Linqing represents a small city, with a population of less than half a million. Therefore, the comparison among these three cities enables us to better understand the influence of urban effects on the winter wheat RGUD across cities with different sizes.

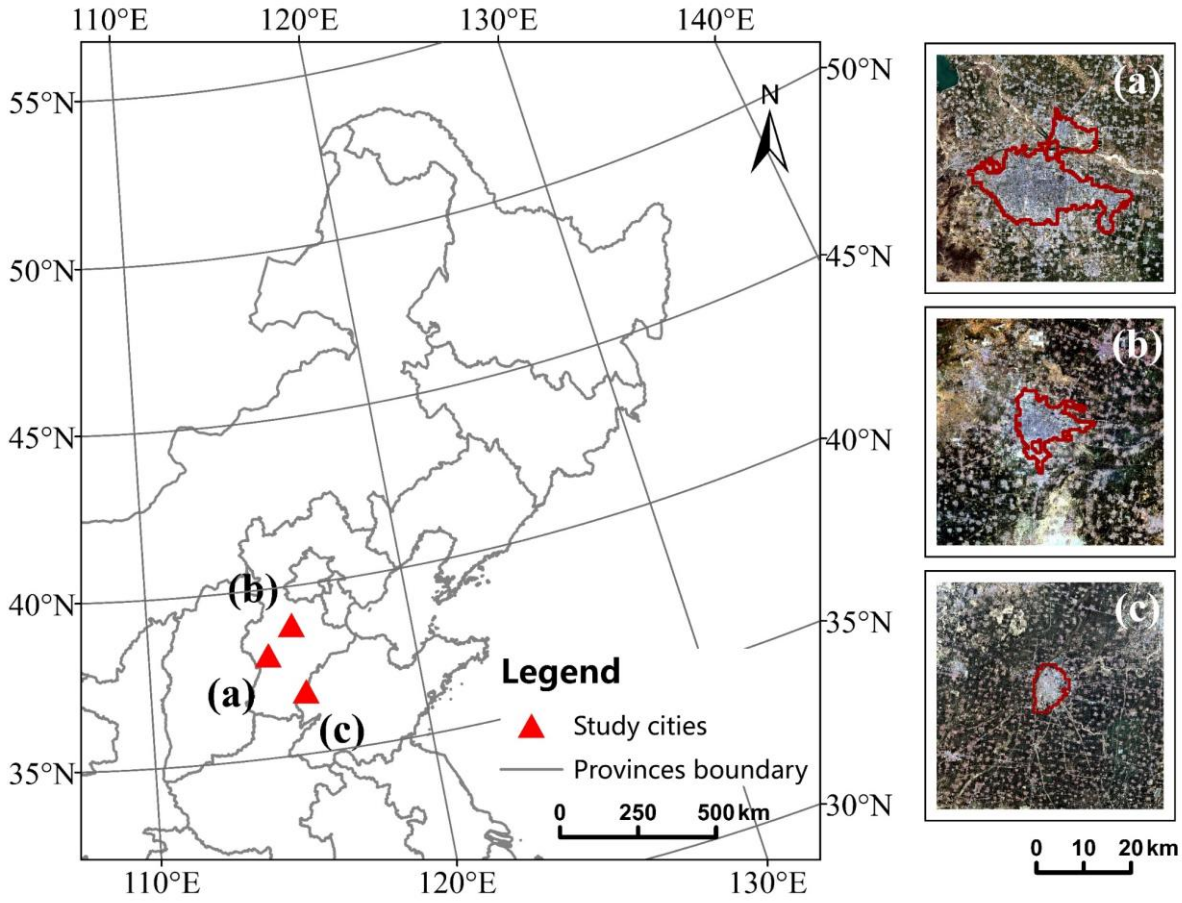

Figure 2. Locations of the three selected cities in northern China and their urban extents (red line) extracted from nighttime light data: (a) Shijiazhuang, (b) Baoding and (c) Linqing. Background image is corresponding Sentinel-2 True Color imagery.

2.2. Dataset

142 The data used in this study include Sentinel-2 images, National Polar-orbiting
143 Partnership visible infrared imaging radiometer suite (NPP-VIIRS) nighttime light data,
144 and MODIS land surface temperature (LST) products.

145

146 *(1) Sentinel-2 Images*

147 Sentinel-2, an advanced optical satellite system for earth observations, offers free
148 multispectral images at 10 m, 20 m, and 60 m spatial resolutions with a 5-day repeat cycle
149 (ESA, 2015). Since Sentinel-2 was launched in 2015, we can collect Sentinel-2 images
150 covering five complete growth cycles of winter wheat, i.e., October 2015 - June 2016,
151 October 2016 - June 2017, October 2017 - June 2018, October 2018 - June 2019 and October
152 2019 - June 2020, according to the winter wheat phenology in north China (Lu et al., 2014;
153 Xiao et al., 2013). We compared the cloud cover ratios and data availability of all Sentinel-
154 2 L1C images from USGS EarthExplorer (https://earthexplorer.usgs.gov) during the
155 above-mentioned five winter wheat growing cycles at three study cities (Figure 3). The
156 winter wheat growth cycle of October 2017 - June 2018 has the largest number of available
157 Sentinel-2 L1C images（less than 20% cloud cover）and the dates of these images have
158 relatively even distribution. A large number of available images can ensure the accuracy
159 and reliability of phenology detection, especially for the second growth stage of winter
160 wheat growth trajectory applied to define RGUD. Besides, after investigation of the
161 multi-year air temperature and precipitation records from meteorological stations, as
162 well as the large-scale vegetation growth status from MODIS images (details are given in
163 the Supplementary Data), we can confirm that October 2017 - June 2018 is not an
164 anomalous period. Therefore, we selected Sentinel-2 images from October 2017 - June
165 2018 for this study. A total of 76 images with less than 20% cloud cover were used to
166 generate dense seasonal time series from which the winter wheat phenology for the three

cities was extracted. Each city has 23-27 images, which provides enough clear observations from the Sentinel-2 images to capture the growth process of winter wheat.

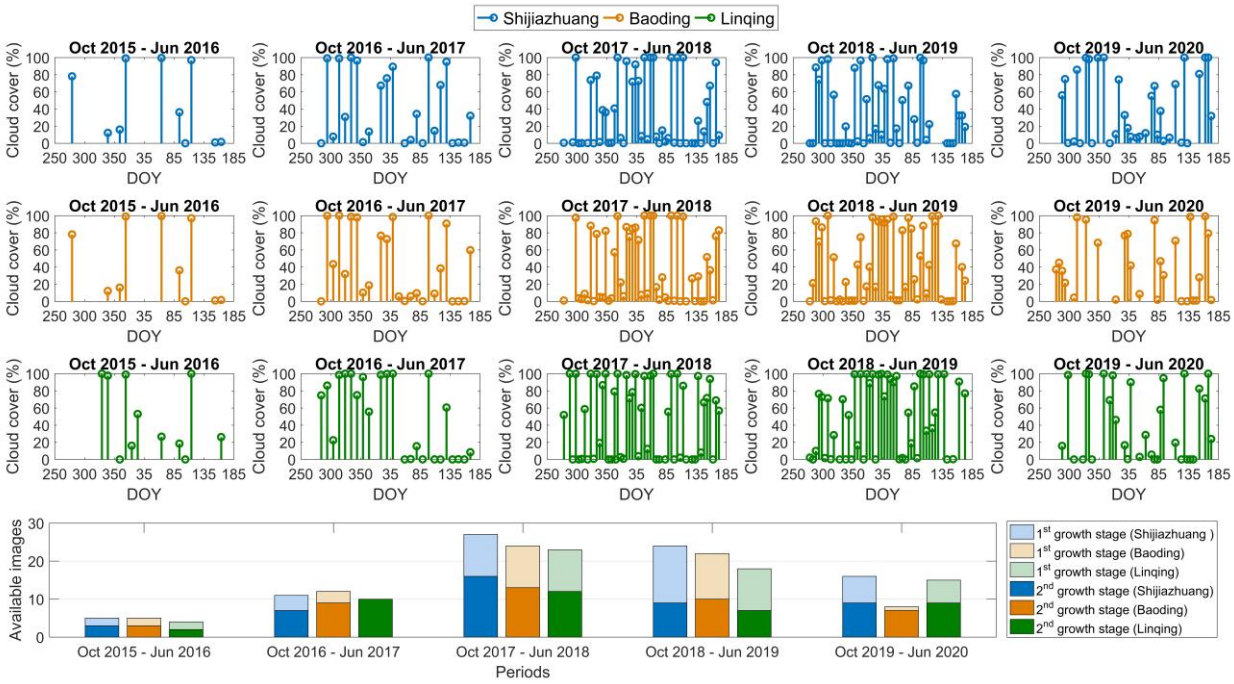

Figure 3. Cloud cover of Sentinel-2 L1C images during October 2015 to June 2020 for each city: Shijiazhuang (T50SKH), Baoding (T50SLH&T50SLJ) and Linqing (T50SLF). The bars indicate the number of Sentinel-2 L1C available images (less than 20% cloud cover) in five winter wheat growth cycles at three study cities. The 1st growth stage of winter wheat means from the seeding to winter dormancy (October to January of the next year) while the 2nd growth stage is from regreening to maturity (February to June).

(2) NPP-VIIRS Nighttime Light Data

The NPP-VIIRS day/night band (DNB), a panchromatic band, can be used to monitor earth's surface nighttime lights because of its ability to sense visible and near-infrared (NIR) wavelengths (Cao et al., 2017). Compared with other nighttime light imagery, such as the Defense Meteorological Satellite Program/Operation Line-Scan (DMSP/OLS), NPP-VIIRS nighttime light images have a higher spatial resolution (750 m) and better

183 performance for monitoring urban dynamics (Ou et al., 2015; Shi et al., 2014b). In this
184 study, to define the urban extent of each city, an annually-averaged nighttime light image
185 was generated using data from October 2017 to June 2018 for tile 3 (75N060E) of the NPP-
186 VIIRS DNB dataset, which was downloaded from
187 https://ladsweb.modaps.eosdis.nasa.gov/search/.

188

189 *(3) MODIS Land Surface Temperature Product*

190 The MODIS LST product is able to model UHI intensity, especially for nighttime LST (Lac
191 et al., 2013; Li et al., 2018; Qiao et al., 2013), with errors within ± 2 K according to ground
192 validation sites (Wan, 2014). MOD11A1 is a daily MODIS LST product with a spatial
193 resolution of 1 km from which the contaminated LST pixels have been removed. In this
194 study, nighttime LST data from MOD11A1 were used to compute the cumulative
195 temperature of winter wheat cultivation sites pre-RGUD. Two tiles (h26v05 and h27v05)
196 of MOD11A1 images were downloaded from
197 https://ladsweb.modaps.eosdis.nasa.gov/search/ to cover the study area.

198

199 ## *2.3. Methodology*

200 As illustrated in Figure 4, this study has five major steps: (1) generating smooth NDPI
201 time series, (2) detecting winter wheat planting areas by a multi-hierarchical classification
202 method, (3) extracting the winter wheat RGUD, (4) extracting the urban extents and
203 buffer zones, and (5) analyzing the winter wheat RGUD patterns in the different buffer
204 zones surrounding the urban areas.

205

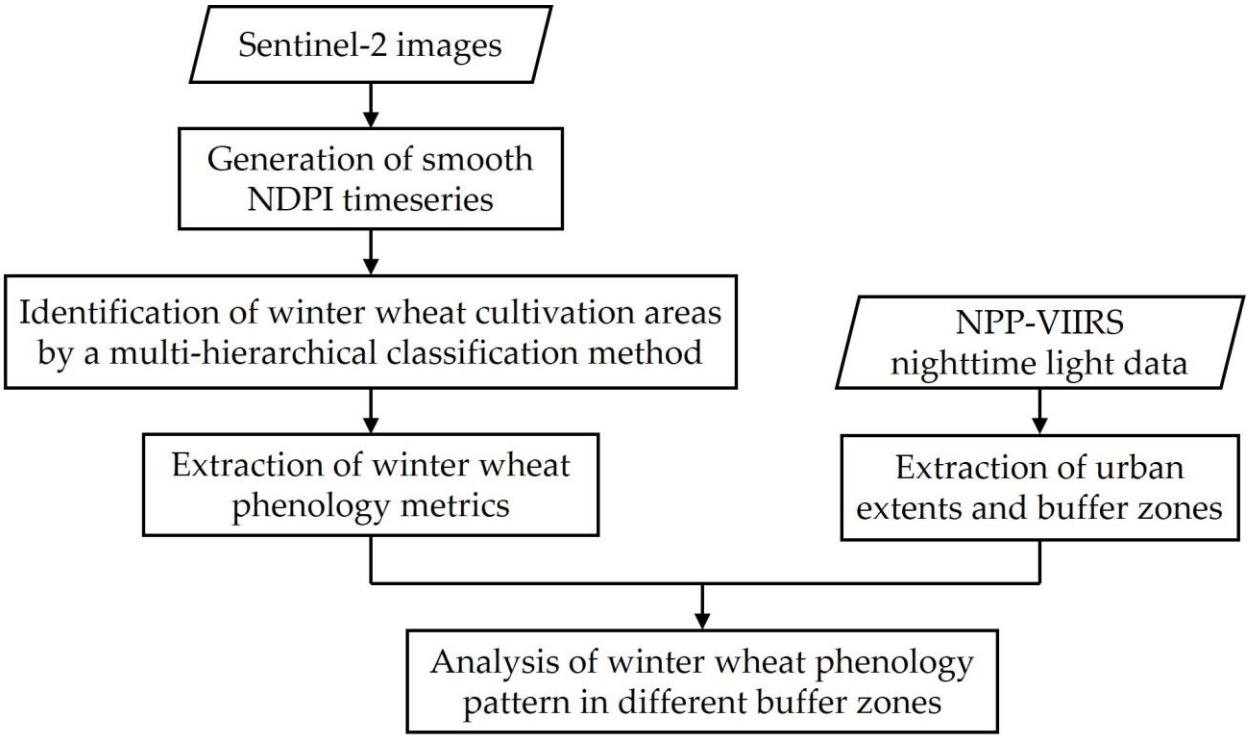

Figure 4. A flowchart of the steps in this study

2.3.1. Generation of a Smooth NDPI Time Series

In this study, NDPI, a three-band vegetation index, was selected to extract winter wheat spring regreening phenology because it is insensitive to the soil and snow background; moreover, it has been shown that NDPI has better performance and superiority than those of other vegetation indexes (e.g., NDVI, EVI and EVI2) for monitoring spring phenology (Wang et al., 2017) and capturing the greenness signal of winter wheat (Dong et al., 2020). There are five substeps to generate smooth NDPI time series. The 1st step is atmospheric correction. Sentinel-2 L1C multispectral images have been geometrically and radiometrically corrected but are available for download without atmospheric correction (ESA, 2015). Therefore, we used the official Sen2cor software to convert Sentinel-2 L1C to L2A, an orthoimage bottom-of-atmosphere corrected reflectance product (Manual, 2018). The 2nd step is screening cloudy pixels. Cloudy pixels were flagged by the Sentinel-CLD

(cloud confidence) band, with values ranging from 0 (clear sky) to 100 (clouds) (Louis, 2017). The Sentinel-CLD band consists of three levels: low (below 35%), medium (35% to 65%) and high (above 65%) cloud probability (Main-Knorn et al., 2015). After visual inspection of the actual images, we defined the pixels with cloud confidence less than 35% as noncontaminated pixels. The 3rd step is to calculate the NDPI time series using the near-infrared (NIR), red and short wavelength infrared (SWIR) bands of the Sentinel-2 L2A images, which have a spatial resolution of 20 m (Equation (1)).

$$\boldsymbol{NDPI} = \frac{\boldsymbol{\rho_{NIR}} - (\boldsymbol{\alpha} \times \boldsymbol{\rho_{red}} + (\mathbf{1} - \boldsymbol{\alpha}) \times \boldsymbol{\rho_{SWIR}})}{\boldsymbol{\rho_{NIR}} + (\boldsymbol{\alpha} \times \boldsymbol{\rho_{red}} + (\mathbf{1} - \boldsymbol{\alpha}) \times \boldsymbol{\rho_{SWIR}})} \quad (1)$$

where, $\boldsymbol{\rho_{NIR}}$, $\boldsymbol{\rho_{red}}$ and $\boldsymbol{\rho_{SWIR}}$ are the surface reflectance at Sentinel-2 band 8 (NIR), band 4 (red) and band 11 (SWIR), respectively, and the weight value ($\boldsymbol{\alpha}$) was set to 0.78, the recommended optimal value that has been validated for Sentinel-2 images (Chen et al., 2019). The 4th step is to interpolate the original NDPI time series to a new time series with an interval of 5 days using the spline interpolation method. The 5th step is to smooth the NDPI time series using the enhanced Savitzky–Golay (SG) filter algorithm (Chen et al., 2004). The enhanced SG filter is one of the most common smoothing methods used to filter contaminated values (e.g., cloud, cloud shadow and noise) from vegetation index profiles, and it has been demonstrated that data smoothed by the SG filter have high similarity with ground observations (Cai et al., 2017; CHU et al., 2016; Han and Xu, 2013).

2.3.2. Hierarchical Classification to Identify Winter Wheat Cultivation Areas

To identify accurate winter wheat cultivation areas, a hierarchical classification method was proposed and used. It consists of two hierarchies. The 1st hierarchy is used to obtain an initial cropland map based on a method combining both pixel- and object-oriented classification results, and the 2nd hierarchy uses curve similarity matching to extract pure winter wheat pixels.

(1) 1st Hierarchy for Detecting All Cropland Types

Traditionally, pixel-oriented and object-oriented methods have been widely used for the classification of remotely sensed imagery (Yan et al., 2006; Zhou et al., 2016). Pixel-oriented classification is based on information (both spectral and temporal) in the individual pixels. For example, the maximum likelihood classification, which assigns pixels to classes based on their probability of belonging to a particular class, is one of the most common pixel-oriented classification methods (Sisodia et al., 2014). Object-oriented classification has the advantage of extracting the attributes of segmented objects and is focused on the characteristic information of image objects, such as texture and spatial features (Benz et al., 2004). Because cropland has unique spectral, temporal, and textural characteristics compared those of other land cover types (e.g., built-up, natural vegetation, water body and soil), we applied both pixel- and object-oriented approaches to classify the Sentinel-2 images into broad land cover types and then selected the intersection of the cropland class in both results as the final cropland map to increase the reliability of cropland detection.

(2) 2nd Hierarchy for Detecting Winter Wheat

The cropland detected by the 1st hierarchical classification should be further refined by the cross correlogram spectral matching (CCSM) method (Chen et al., 2016; Wang et al., 2009). First, we manually selected pure winter wheat pixels, referring to high-resolution images in Google Earth, and calculated the average values of these pixels as reference winter wheat NDPI profiles. Then, the NDPI profiles of the other cropland pixels were regarded as the target NDPI profiles to be judged by CCSM similarity, as shown in Figure 5 (a). Then, the similarity between the target NDPI profiles and the reference NDPI profile was measured by the CCSM method. Specifically, the target NDPI profile moves to

different positions to find a match (i.e., forward and backward up to 25 days, with 5 days per step). Then, a correlation coefficient (Rm) was calculated between the reference winter wheat NDPI profile and each target NDPI profile at different matching positions (Wang et al., 2009) (Equation (2)):

$$R_m = \frac{n\sum \lambda_r \lambda_t - \sum \lambda_r \lambda_t}{\sqrt{\left[n\sum \lambda_r^2 - (\sum \lambda_r)^2\right]\left[n\sum \lambda_t^2 - (\sum \lambda_t)^2\right]}} \quad (2)$$

Here, λ_r, and λ_t are the reference winter wheat NDPI profile and target NDPI profile, respectively, and n is the number of overlapping positions. The largest Rm value selected from all the matching positions, as shown in Figure 5 (b), was used to judge whether the target pixel was planted as winter wheat. Since winter wheat is the target of our study, the user's accuracy of winter wheat mapping is a significant metric for the control of the errors and uncertainty in the following analysis. As a result, in this study, the upper threshold of Rm was set to 0.9 to ensure the accuracy of the selected winter wheat pixels. The upper Rm threshold implies a highly similar temporal pattern between the target pixels and the reference profile. In other words, the 2nd hierarchical refinement can not only exclude nonwinter-wheat cropland pixels but also remove pixels of mixed crops, which guarantees the rationality of the following analysis when using this strict procedure. Figure 6 shows the winter wheat mapping results for the three cities.

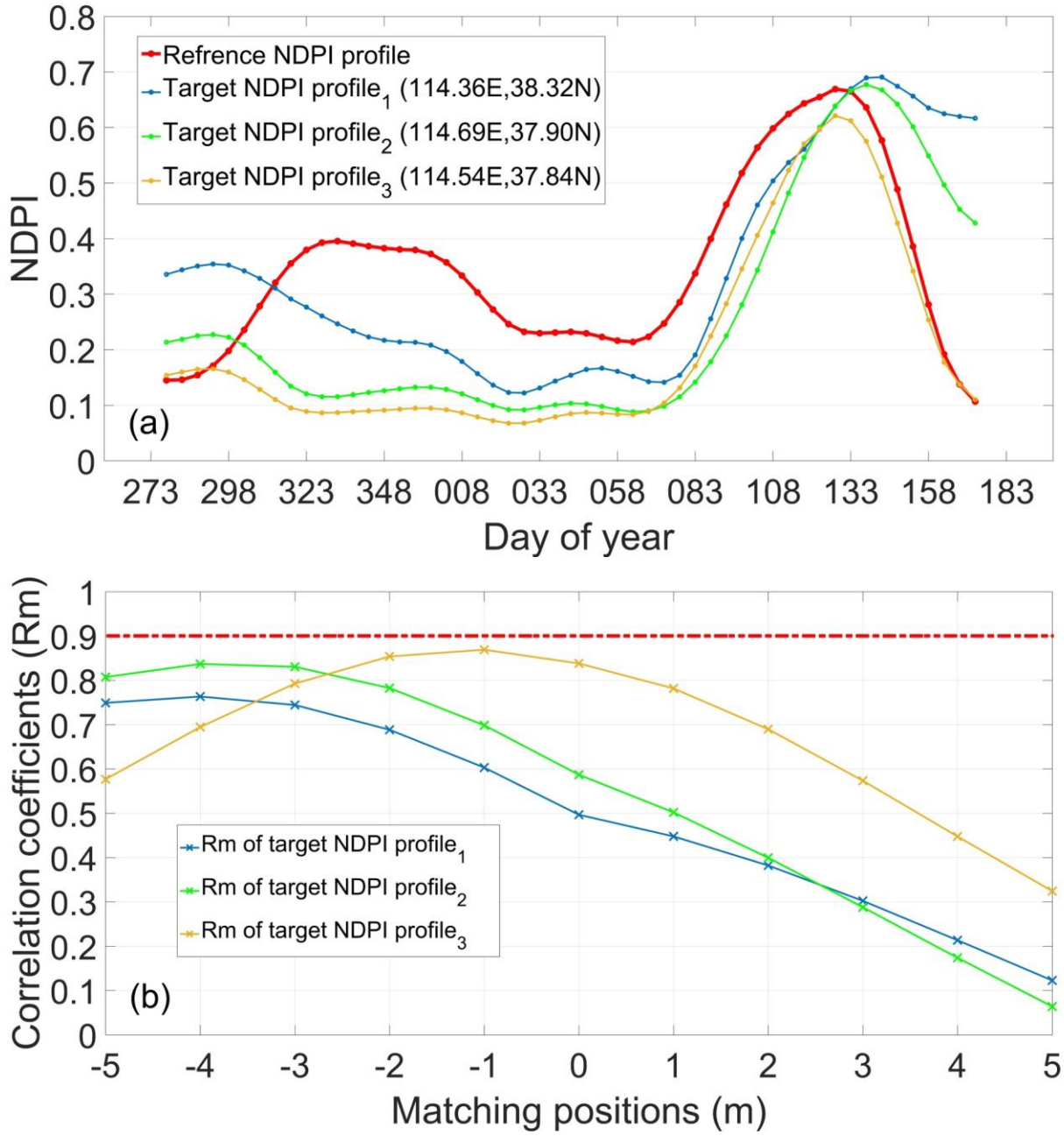

289

290

291

292 **Figure 5.** (a) Reference winter wheat NDPI profile and target NDPI profiles to be judged

293 by CCSM similarity; (b) correlation coefficient (Rm) of the three target NDPI profiles at

294 different matching positions

295

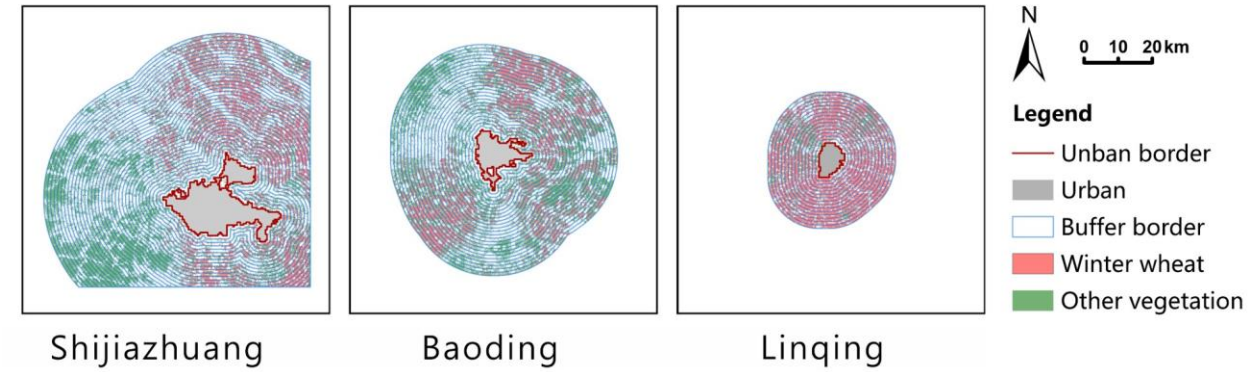

Figure 6. Winter wheat maps and buffer zones of Shijiazhuang, Baoding and Linqing

2.3.3. Winter Wheat Spring Regreening Phenology Extraction

The NDPI profile of winter wheat clearly shows two main phases of development during its life cycle (Figure 7). Numerous studies have focused on the second phase of development (i.e., a period covering winter wheat regreening, heading and harvesting dates and the development of reproductive organs) owing to its significance (CHU et al., 2016; Liu et al., 2016; Lu et al., 2014). Specifically, the RGUD begins when winter wheat is regrowing after being dormant in the winter. It is also a key period for promoting the growth of late-emerging, weak seedlings, controlling the length of the seedling stage, regulating the size of the population and determining the rate of ear formation. In the NDPI profile, the spring RGUD was defined as the date of year (DOY) since January 1, 2018, when the NDPI value reached 20% of the magnitude of the 2nd growth stage (CHU et al., 2016; Yao et al., 2017), as shown in Figure 7.

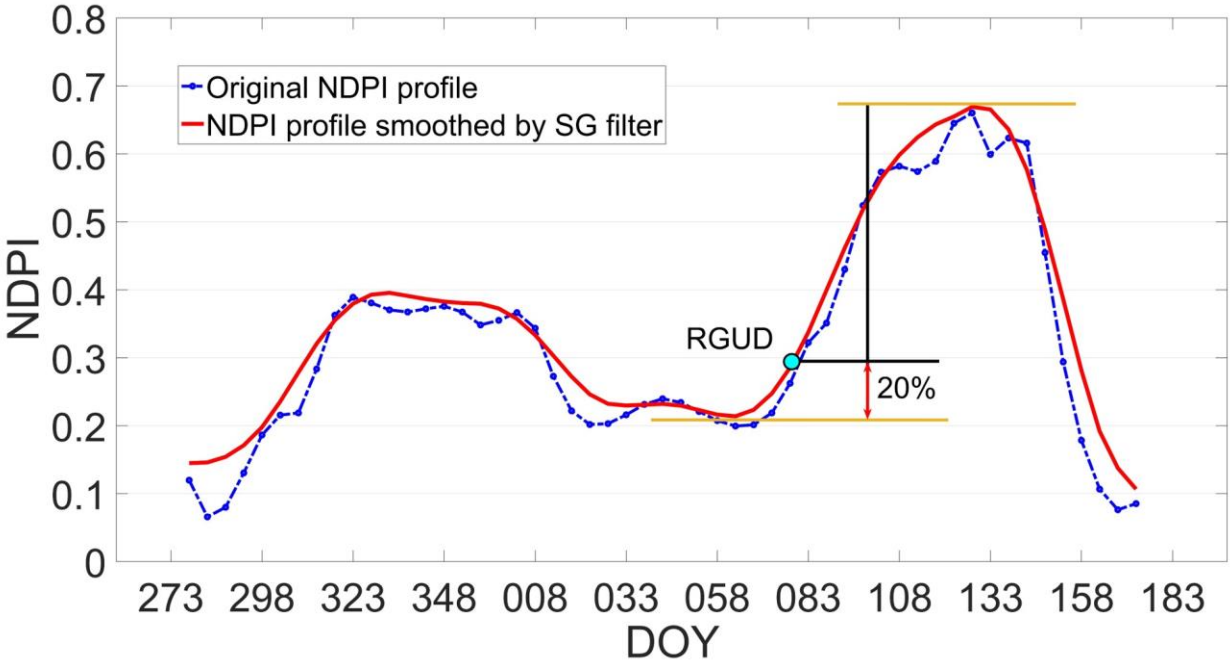

Figure 7. Extraction of the winter wheat RGUD from the NDPI profile according to the relative threshold method

2.3.4. Urban Extent and Buffer Zone Extraction

First, an annual NPP-VIIRS nighttime light image was calculated by averaging the monthly light images within the winter wheat growth cycle, and then the urbanized area of the three cities was extracted from the annual nighttime light image based an optimal threshold: Shijiazhuang & Baoding, NPP-VIIRS DN=10 nanowatts/(cm2·sr); Linqing, NPP-VIIRS DN=5 nanowatts/(cm2·sr) (Shi et al., 2014a). In addition, to capture the smooth boundaries of the main urban areas, isolated bright areas far from the urban center are manually excluded and corrected by manual inspection according to the urban built-up area scope in Google Maps. After defining the urban extent of each city, 35, 25, and 15 buffer zones with a 1 km interval from the urban boundaries were created for Shijiazhuang, Baoding, and Linqing, respectively, to represent subregions with different

distances to the urban areas (Figure 6) because areas affected by UHIs increase with urban size (Imhoff et al., 2010).

2.3.5. Analysis of RGUD Spatial Distribution and Driving Factors

The RGUD was visualized in the buffers of the three cities to show the spatial distribution patterns. To explore the driving factors of the RGUD spatial distribution, the 1 km MODIS nighttime LST product was used to calculate the cumulative temperature in the test period from the average NDPI minimum date to the average winter wheat RGUD. Then, the winter wheat pixels (20 m) were aggregated into 1 km pixels to match the resolution of the preregreening cumulative temperature data (1 km). The relationship between the RGUD and cumulative temperature was quantified by linear regression. Next, the urban effect on winter wheat RGUD was analyzed at the buffer scale for each city. First, the mean and standard deviation of the winter wheat RGUD in each 1 km width buffer zone was calculated. Subsequently, the mean phenological features of the buffers were plotted against the distance to the urban boundary to visualize the relationship between phenology and urban areas. Furthermore, a linear regression was conducted to quantify how urban areas affect winter wheat RGUD at different distances.

3. Results

3.1 Spatial Distribution of Winter Wheat RGUD

Figure 8 shows the spatial distributions and histograms of the frequency of the winter wheat spring RGUD in the three cities. The outliers that are outside of 3-sigma standard deviations have been excluded. In general, the winter wheat RGUD in the surroundings of the urban areas of each city show normal distributions, and the RGUD occurs earlier close to the urbanized areas of each city. In addition, the average regreening dates are

76.41 in Linqing (36° 50' 27"N), 81.04 in Shijiazhuang (38° 02' 34"N) and 84.16 in Baoding (38° 51' 21"N), suggesting that re-greening dates of winter wheat in lower latitudinal regions (i.e., warmer areas) generally occur earlier. This implies that temperature may be the key driver factor to control winter wheat spring phenology at large scales, which are consistent with studies on other vegetation (He et al., 2015; Piao et al., 2011). The difference in average RGUD values of these three cities also suggests that the method and data used by this study to detect winter wheat RGUD is reasonable and reliable.

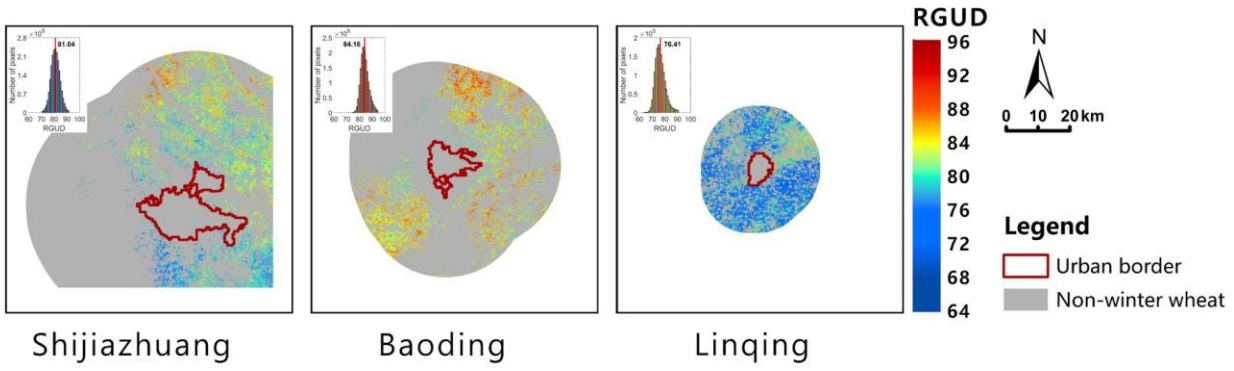

Figure 8. Spatial distribution of the winter wheat RGUD in the buffer zone of three cities. The histograms on the upper left of maps show the number of pixels with different winter wheat RGUD values in each city; the red lines in histograms indicate the average winter wheat RGUDs in each city.

3.2 Relationship between Winter Wheat RGUD and Nighttime LST

We can see from the histogram distributions of nighttime LST (Figure 9) and statistics of nighttime LST (Table 1) across the cities that the nighttime LST can be a good metric to describe urban sizes; the larger the city, the larger the difference in nighttime LST and the higher the standard derivation. In addition, as shown in Figure 9, the scatter plots present a negative correlation between winter wheat RGUD and nighttime LST in each city, which indicates that high nighttime LST might drive earlier winter wheat spring RGUDs.

Interestingly, large- and middle-scale cites have higher correlation coefficients (r), i.e., -0.64 in Shijiazhuang ($p < 0.01$) and -0.51 in Baoding ($p < 0.01$), than that in the small city Linqing (r: -0.08, $p < 0.01$).

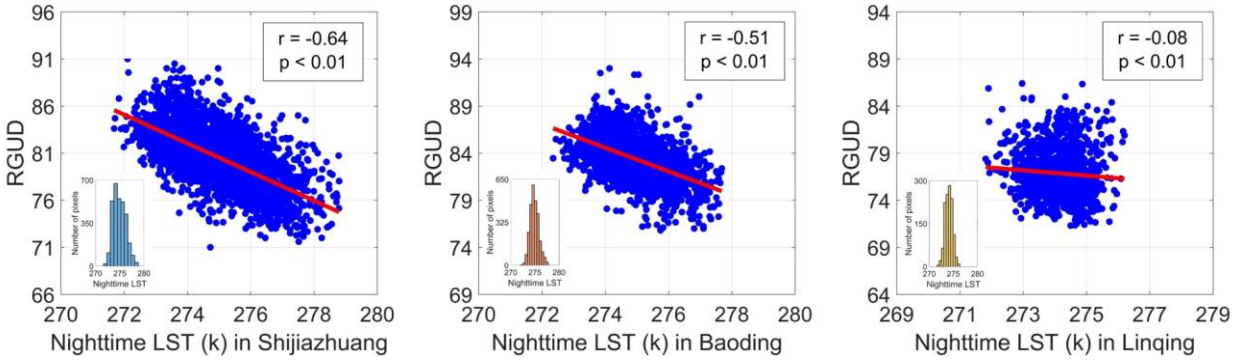

Figure 9. Relationship between the nighttime LST and winter wheat RGUDs. The blue point presents the RGUD value of one pixel and its corresponding nighttime LST value. Lower-right figure in each scatter plot is the histogram of the nighttime LST in each city.

Table 1. Statistics of the nighttime LST across the cities; the outliers (based on 3-sigma standard deviations) have been screened

Study Site	Range (k)	Nighttime LST Difference	Average	STD
Shijiazhuang	273.12 - 277.16	4.04	274.91	1.28
Baoding	273.55 - 276.52	2.97	274.89	0.89
Linqing	272.90 - 275.27	2.37	274.03	0.74

3.3 Winter Wheat RGUD Change along the Urban-rural Gradient

To summarize both the LST and RGUD in the 1 km buffers, we resampled the MODIS nighttime LST (1 km) into 20 m pixels using the bilinear method. The orange dots and lines in Figure 10 show the average nighttime LST in each 1 km buffer zone. Obviously, the UHI effect decreases from the urban centers to the surrounding areas in all the study cities. The UHI in the large city, Shijiazhuang, has the most significant warming effect on

the surrounding area, while the small city, Linqing, experiences the weakest effect. As expected, in general, all three cities show earlier winter wheat RGUDs when closer to the urbanized area, but the specific patterns are different among the cities (Figure 10). For the large city, Shijiazhuang, we found three stages of winter wheat RGUD change with distance to the urbanized area: (1) The winter wheat RGUDs in the 11 buffer zones closest to the urbanized area show stable advancement, as shown in Figure 10. The winter wheat in these areas has similarly early RGUDs (approximately 79 DOY). (2) After the first 11 buffer zones, there is a significant increasing trend in the RGUD (0.26 day/km, as shown in Table 2), indicating that winter wheat enters spring phenology later when farther from the urbanized area. This increasing trend stops at 27 km. (3) When farther than 27 km from the urban areas, the winter wheat RGUD becomes stable again, but with a late date of approximately 84 DOY. There also exists a stable advancement of the winter wheat RGUD (approximately 81 DOY) in the middle of Baoding, but with a much shorter range, i.e., within 3 km of the urbanized areas, as shown in Figure 10. In contrast, the winter wheat RGUD of the small city, Linqing, does not have a stable advancement stage, such those in as Shijiazhuang and Baoding, but it shows an increasing trend starting from the first buffer zone, as shown in Figure 10. The change rates of the middle and small cities are 0.21 day/km and 0.11 day/km (Table 2), respectively, which are smaller than those of Shijiazhuang, suggesting that the urban warming effect may decline towards the outskirts more slowly in small cities than it does in large cities. In addition, the increasing trend of the winter wheat RGUD in Baoding and Linqing stops in the buffer zone (14 km and 7 km), which is closer to the urban areas than that of Shijiazhuang (27 km), suggesting that the effect of small cities on winter wheat RGUD has a shorter range than that of large cities.

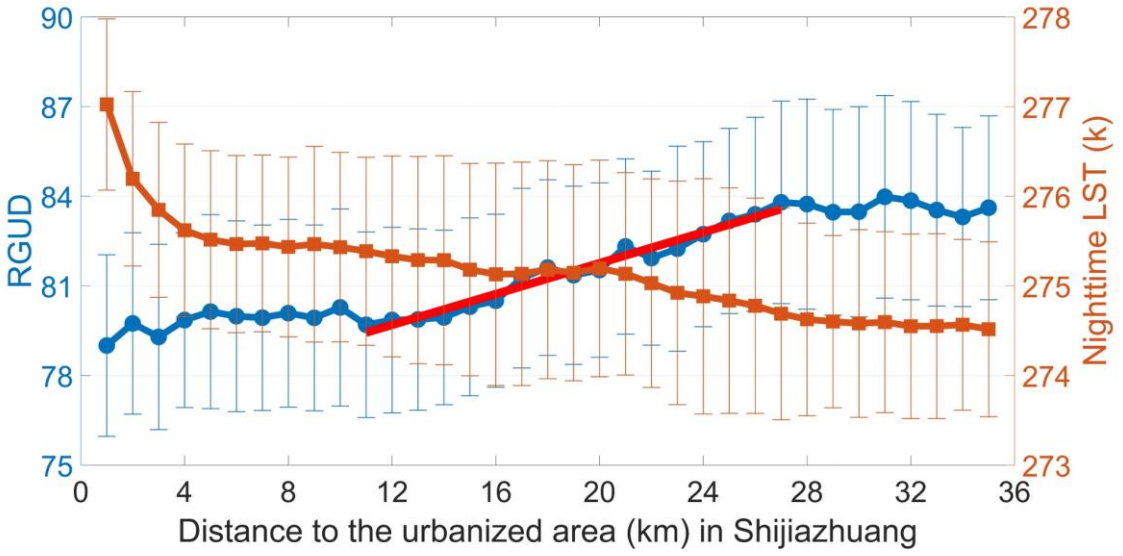
RGUD
Nighttime LST (k)
Distance to the urbanized area (km) in Shijiazhuang

415

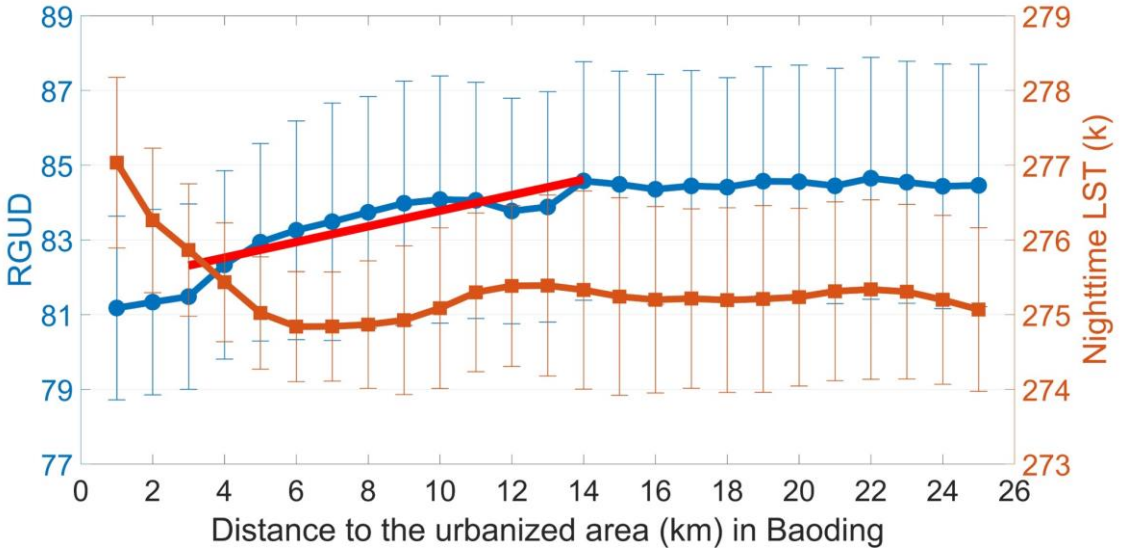
RGUD
Nighttime LST (k)
Distance to the urbanized area (km) in Baoding

416

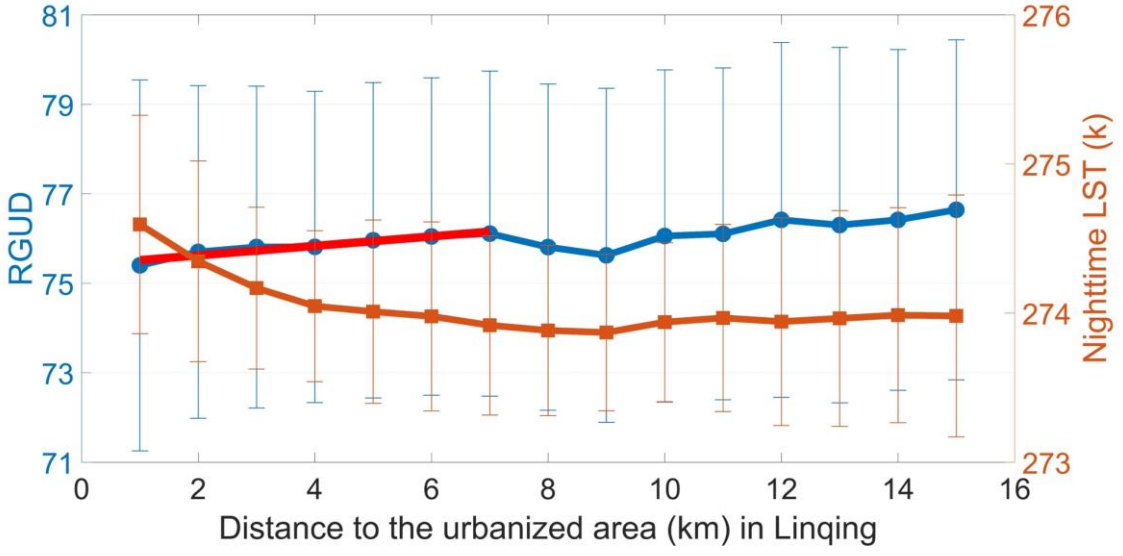
RGUD
Nighttime LST (k)
Distance to the urbanized area (km) in Linqing

417

Figure 10. Relationship between the distance to the urbanized area and winter wheat RGUD in each city; the red lines indicate the fitted lines

Table 2. Summary of the linear regression between the RGUD and distance to the urbanized area

Study site	Affected range (km)	Regression range (km)	Slope	r	p-value
Shijiazhuang	01 - 27	11 - 27	0.26	0.98	<0.01
Baoding	01 - 14	03 - 14	0.21	0.88	<0.01
Linqing	01 - 07	01 - 07	0.11	0.96	<0.01

4. Discussion

4.1 Impact of Urban Size on Winter Wheat RGUD

There are minimum temperature requirements for vegetation (e.g., root and leaves) development (Basler et al., 2016; Schenker et al., 2014). Both satellite-based remote sensing data and ground observations suggest that vegetation spring phenology occurs earlier along the urban-rural gradient, and it occurs much earlier when close to the urban center because of the UHI effect, which causes higher temperatures (Dallimer et al., 2016; Li et al., 2016; Yao et al., 2017; Zhao et al., 2014). This study not only validated this phenomenon, but also found that no matter what the size of a city is, i.e., Shijiazhuang, Baoding or Linqing, winter wheat spring RGUD occurs earlier when close to an urban center. In addition, we provided further insights into how winter wheat RGUD responds to the temperature gradient in urban-rural areas among cities of different sizes. Specifically, in addition to considering the winter wheat phenological differences between nearby urban areas and outskirts, we hope to recognize the interaction between

the RGUD and urban areas in each buffer through the design of buffer zones for different-scale cities (Figure 6). In this regard, we controlled several factors that might affect vegetation spring phenology, such as external factors (e.g., photoperiod, precipitation and temperature caused by latitudinal climate zones) and internal factors (e.g., vegetation species), by selecting a single species (i.e., winter wheat) and cities of different sizes located in the same climate zone. This improvement is based on previous studies in which uncertainties were included. For example, previous studies have concentrated on major cities with similar scales to evaluate urban effects on mixed vegetation phenology by moderate-coarse satellite images (Ren et al., 2018; Zhou et al., 2016). Thus, in this study, we assumed that differences in the winter wheat RGUD are mainly due to the urban-induced microclimates of cities with different sizes.

Figure 11 shows the difference in the advancement of the winter wheat RGUDs between each buffer and the furthest affected buffer zone (i.e., the 27th zone for Shijiazhuang, the 14th for Baoding and the 7th for Linqing) in the three cities. This indicates that the urban effects on the winter wheat RGUD are different for different-scale cities: the larger the city, the greater the range of the effect, thereby causing a larger advancement of the winter wheat regreening phenology. This phenomenon could be explained by the Fick's first law of diffusion that describes relationship between diffusive flux and concentration, that is, the flux moves from high to low concentration regions, and its magnitude is proportional to the concentration gradient. Large city has higher urban-rural heat flux (i.e., nighttime LST) difference than middle- and small-scale cities (Table 2), which causes greater RGUD advancement in larger city. Moreover, following Fick's first law of diffusion, larger cities with higher heat gradients exchange at a faster rate than that of smaller cities, which causes change rate of the RGUD along the urban-rural gradient is significantly higher in the large city (Shijiazhuang: 0.26 day/km) than it is in the middle- and small-scale cities (Baoding: 0.21 day/km and Linqing: 0.11 day/km) (Figure 10 and

Table 2). Thus, combined with Figure 10 and Figure 11, our results confirm the abovementioned hypothesis; that is, variability in the increasing temperature along urban-rural gradients could affect winter wheat spring regreening phenology in the surrounding urban areas, and the strength of this effect is tightly correlated with urban sizes. Although higher temperatures generally result in earlier spring phenology, vegetation spring phenology does not necessarily occur earlier with increasing temperature because green-up may respond to temperature nonlinearly and be saturated at high temperature (Caffarra et al., 2011). Here, we found stable advancement stages of the winter wheat RGUD in larger cities, i.e., Shijiazhuang (1-11 km) and Baoding (1-3 km), while the small city, Linqing, does not have a stable advancement stage (Figure 11). The stable advancement stage of winter wheat RGUD indicates that the accumulated temperature required for winter wheat spring regreening reaches saturated conditions and a further increase in temperature will not trigger earlier spring regreening phenology in areas close to large cities. In these areas, other factors may constrain the regreening of winter wheat, e.g., shorter photoperiods limit leaf development (Chmielewski and Götz, 2016; Garonna et al., 2018).

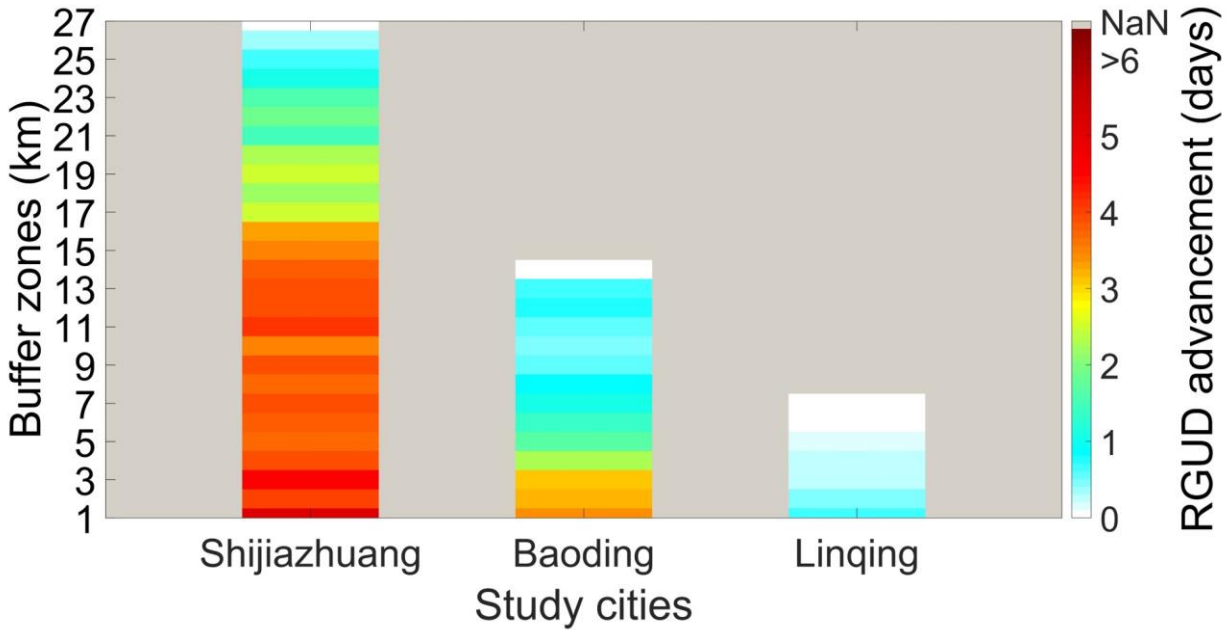

Figure 11. Comparison of the advanced winter wheat RGUD across the cities

4.2 Possible Mechanism of the Urban Effect on the Winter Wheat RGUD

Nighttime LST is a good indicator of UHIs (Lac et al., 2013; Land et al., 2016; Li et al., 2018), and it can be regarded as one of the key drivers of vegetation spring phenology, i.e., there is a negative correlation between vegetation spring phenology and nighttime LST (X. Wang et al., 2017; Zhou et al., 2016). We found that the relationship between winter wheat spring regreening and nighttime LST, indeed, shows a negative correlation in each city, but it differs by urban size, i.e., the smaller the city is, the weaker the correlation is. In general, the UHI effect intensity depends on urban size and building density, with larger cities having stronger UHI effect intensities. Therefore, due to the larger UHI effect intensity, Shijiazhuang and Baoding show a higher correlation between nighttime LST and vegetation spring phenology than that of Linqing. Specifically, the UHI effect is generally defined as thermal or microclimatic differences between urban areas and their surrounding rural areas (Brazel, 2006; Parece and Campbell, 2018). These differences mainly result from the replacement of natural landscapes with impermeable

surfaces and built up areas (Jochner and Menzel, 2015; Samuel C Zipper and Jason Schatz et al., 2016). More specifically, impervious surfaces increase the local temperature due to the occurrence of less evapotranspiration from a low abundance of vegetation (Jochner and Menzel, 2015). Thus, we extracted the proportions of impervious surfaces in winter wheat pixels in 3x3 windows, and the results are shown in Figure 12.

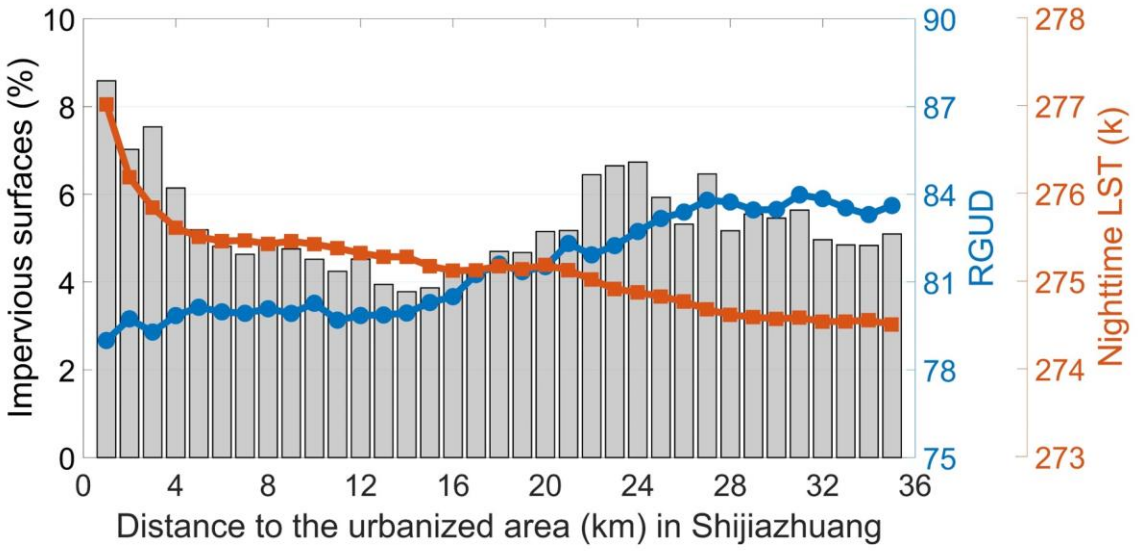

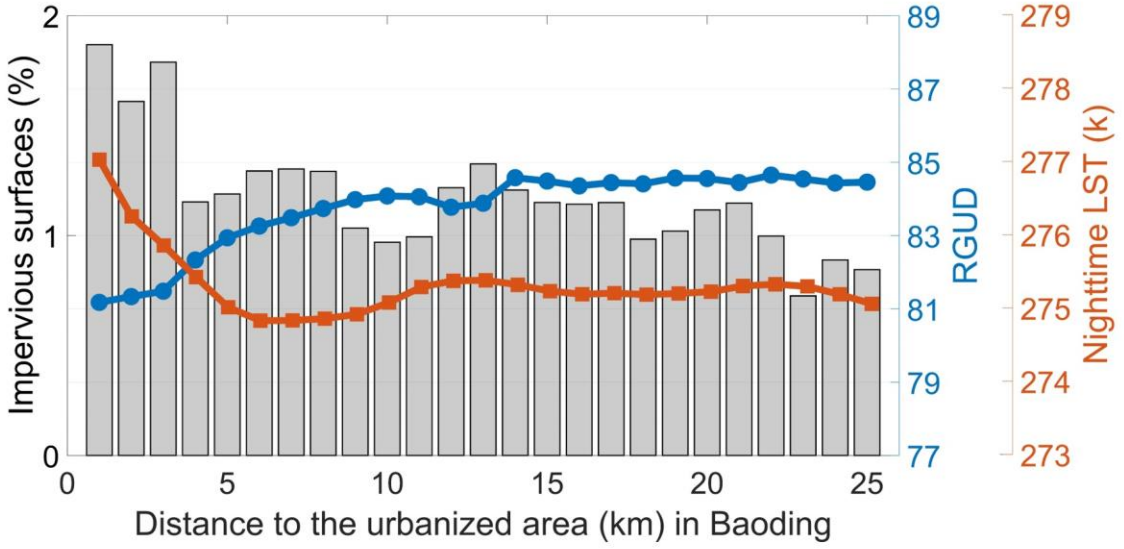

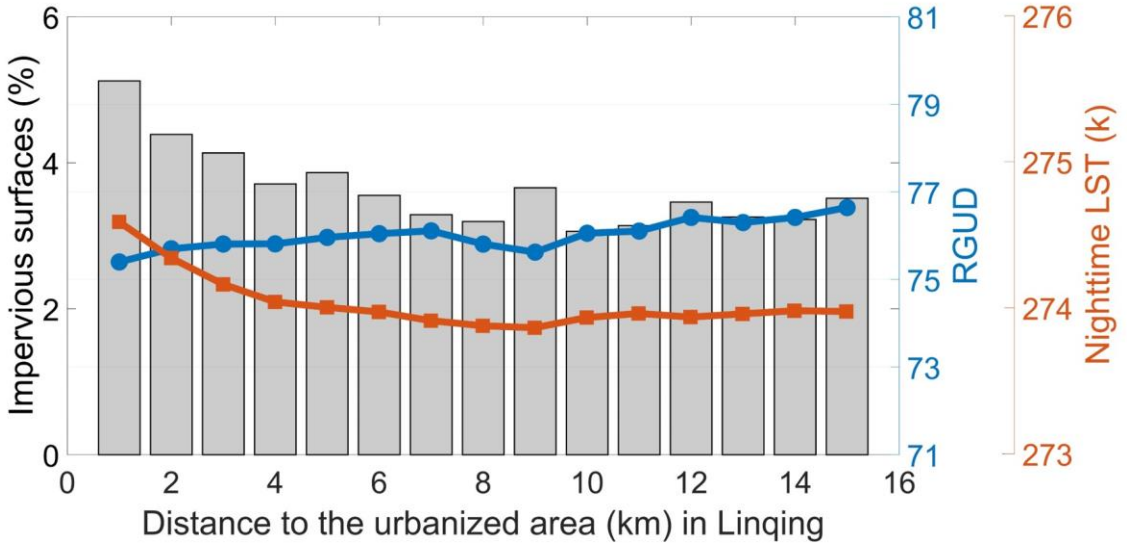

Figure 12. Impervious surfaces proportions surrounding winter wheat

Table 3. Correlation coefficients between the winter wheat regreening date, nighttime LST and proportion of impervious surfaces (**p < 0.01)

Study site	Correlation coefficient between nighttime LST and regreening date	Correlation coefficient between the proportion of impervious surfaces and regreening date
Shijiazhuang	-0.64**	0.05
Baoding	-0.51**	-0.84**
Linqing	-0.08**	-0.66**

According to Figure 12, a higher proportion of impervious surfaces surrounding winter wheat generally make its spring phenology earlier. Additionally, the percentage of impervious surfaces and nighttime LST are more highly correlated in the middle- and small-scale cities (Baoding and Linqing) than they are in the large city (Shijiazhuang). This indicates that the local microclimate in the middle- and small-scale cities is mainly produced by impervious surfaces, which causes the advancement of the winter wheat

519 regreening phenology. By comparison, there is a weak relationship between the
520 proportion of impervious surfaces and winter wheat regreening in Shijiazhuang, yet
521 there is a strong relationship between the nighttime LST and winter wheat regreening
522 (Table 3). One possible reason is the unsynchronized relationship that occurs between the
523 proportion of impervious surfaces and temperature differences (also referred to as UHI
524 intensity) in some cities, but especially in large cities. This is mainly because satellite-
525 based remotely sensed images can capture only the proportions of buildings and
526 construction canopies rather than the actual building heights and density. The
527 impervious layers extracted by satellite images cannot fully reflect the UHI intensity.
528 Similarly, a recent study suggested that vegetation phenology is controlled by both local
529 land cover and micrometeorological conditions and that impervious cover can only
530 partially explain variability in phenology (Samuel C Zipper and Jason Schatz et al., 2016).
531 Other possible reasons for the observed relationship are the much stronger heat
532 convection and flow of higher concentration of pollutants (e.g., CO_2) from the urban-rural
533 areas in large-scale cities. As a recent finding demonstrated, the efficiency of heat
534 convection to the lower atmosphere from urban and rural areas is also significantly
535 responsible for the UHI effect (Zhao et al., 2014). The other study suggested the rise of
536 CO_2 concentration, particularly in urban areas, may change sensitivity of vegetation
537 seasonality resulting in earlier start of season (Wang et al., 2019). Thus, the influential
538 factors for winter wheat regreening might be different in cities with different sizes, i.e.,
539 impervious surface cover influences phenology more significantly in middle- and small-
540 size cities, whereas the influential factors are more complicated and mixed in large cities
541 where impervious surfaces, UHI heat convection, and concentration of pollutants all
542 might play important roles.
543

544 ## 5. Conclusion

Accurate monitoring of key phenology characteristics, such as spring regreening phenology, is critical for yield forecasts and crop management (He et al., 2015; Liu et al., 2018). As previously documented, 40% ~ 60% of irrigated agriculture and rainfed croplands are planted within 20 km of urban areas, so the urban effects on changes in crop phenology could result in a significant influence on food security (Samuel C Zipper and Jason Schatz et al., 2016; Thebo et al., 2014). Based on this, we hypothesized that urban-induced microclimate variability can affect the winter wheat spring phenology and that this effect might vary with urban size. We developed a novel methodology to test this hypothesis. The proposed methodology includes (1) a hierarchical classification method to identify winter wheat cultivation areas, which could exclude misclassification and refine winter wheat planting areas; (2) a workflow to process high-resolution Sentinel-2 time series (20 m), which can reduce scaling and mixed-pixel effects; and (3) a novel 3-band vegetation index (NDPI), which is insensitive to background land cover types and was employed to reflect the annual winter wheat growth trajectory. The abovementioned methodology can accurately classify winter wheat pixels, detect winter wheat RGUDs and reduce uncertainty.

Based on this newly developed methodology, our results showed that the spatial patterns of the winter wheat RGUDs are similar in each city, i.e., there is an earlier winter wheat spring regreening close to the urbanized areas. However, the affected ranges, stable advancement stages and slopes of the winter wheat spring regreening phenology in response to distance from urban areas are different for the cities of different sizes. These differences are probably due to the UHI intensity of the different cities. Larger cities have a larger UHI effect intensity, causing much stronger impacts on winter wheat regreening phenology. Additionally, the urban-induced microclimatic effects on the winter wheat spring regreening phenology depend on urban size, and the response of winter wheat regreening to nighttime LST is more significant in the large city (Shijiazhuang), while the

proportion of impervious surfaces contributes more the in middle- and small-scale cities (Baoding and Lining, respectively).

These results, together with previous agronomy studies highlighting the importance of spring regreening phenology in determining winter wheat growth, suggest that the UHI effect should be considered in studies on phenology monitoring, yield forecasting, and intelligent agricultural management of urban vegetation. Findings from this study can help improve winter wheat yield predictions as well as winter wheat farming practices locally. Moreover, rapid urbanization (the long-term process of transforming a small city into a large city) is occurring globally. In this regard, we selected three cities of differing sizes that are located in the same climate zone to investigate the urban-induced microclimate effects on winter wheat spring regreening phenology. Due to the limited number of cloud-free satellite images, this study only investigated one growing season of winter wheat in three representative cities. The methodology developed by this study can be adopted by future studies to investigate more seasons and cities to test the findings of this study.

Acknowledgements

This study was supported by the National Natural Science Foundation of China (project no.41701378), Research Grants Council of Hong Kong (project no.25222717), and Research Institute for Sustainable Urban Development, the Hong Kong Polytechnic University (project no. 1-BBWD).

Supplementary data

Supplementary data associated with this article can be found, in the online version, at ###

References

Anwar, M.R., Liu, D.L., Farquharson, R., Macadam, I., Abadi, A., Finlayson, J., Wang, B., Ramilan, T., 2015. Climate change impacts on phenology and yields of five broadacre crops at four climatologically distinct locations in Australia. Agric. Syst. 132, 133–144. https://doi.org/10.1016/j.agsy.2014.09.010

Basler, D., Kollas, C., Lenz, A., 2016. Where , why and how◎? Explaining the low-temperature range limits of temperate tree species 1076–1088. https://doi.org/10.1111/1365-2745.12574

Benz, U.C., Hofmann, P., Willhauck, G., Lingenfelder, I., Heynen, M., 2004. Multi-resolution, object-oriented fuzzy analysis of remote sensing data for GIS-ready information. ISPRS J. Photogramm. Remote Sens. 58, 239–258. https://doi.org/10.1016/j.isprsjprs.2003.10.002

Brazel, B.C.H. and A.J., 2006. Arizona-Nevada Academy of Sciences Urban , Residential , and Rural Climate Comparisons from Mobile Transects and Fixed Stations◎: Phoenix , Arizona 38, 77–87.

Caffarra, A., Donnelly, A., Chuine, I., Jones, M.B., 2011. Modelling the timing of Betula pubescens budburst. I. Temperature and photoperiod: A conceptual model. Clim. Res. 46, 147–157. https://doi.org/10.3354/cr00980

Cai, Z., Jönsson, P., Jin, H., Eklundh, L., 2017. Performance of smoothing methods for reconstructing NDVI time-series and estimating vegetation phenology from MODIS data. Remote Sens. 9, 20–22. https://doi.org/10.3390/rs9121271

Cao, C., Xiaoxiong, X., Wolfe, R., DeLuccia, F., Liu, Q. (Mark), Blonski, S., Lin, G. (Gary), Nishihama, M., Pogorzala, D., Oudrari, H., Hillger, D., 2017. NOAA Technical Report NESDIS 142 Visible Infrared Imaging Radiometer Suite (VIIRS) Sensor Data Record (SDR) User's Guide Version 1.3. Noaa. https://doi.org/10.1016/j.nbt.2010.07.010

Chen, J., Jönsson, P., Tamura, M., Gu, Z., Matsushita, B., Eklundh, L., 2004. A simple method for reconstructing a high-quality NDVI time-series data set based on the Savitzky-Golay filter. Remote Sens. Environ. 91, 332–344. https://doi.org/10.1016/j.rse.2004.03.014

Chen, J., Rao, Y., Shen, M., Wang, C., Zhou, Y., Ma, L., Tang, Y., Yang, X., 2016. A Simple Method for Detecting Phenological Change From Time Series of Vegetation Index. IEEE Trans. Geosci. Remote Sens. 54, 3436–3449. https://doi.org/10.1109/TGRS.2016.2518167

Chen, X., Guo, Z., Chen, J., Yang, W., Yao, Y., Zhang, C., Cui, X., Cao, X., 2019. Replacing

633 the Red Band with the Red-SWIR Band Vegetation Indices to Soil Background.
634 Remote Sens. 1–15. https://doi.org/10.3390/rs11070851

635 Chen, X., Wang, D., Chen, J., Wang, C., Shen, M., 2018. The mixed pixel effect in land
636 surface phenology: A simulation study. Remote Sens. Environ. 211, 338–344.
637 https://doi.org/10.1016/j.rse.2018.04.030

638 Chmielewski, F.M., Götz, K.P., 2016. Performance of models for the beginning of sweet
639 cherry blossom under current and changed climate conditions. Agric. For. Meteorol.
640 218–219, 85–91. https://doi.org/10.1016/j.agrformet.2015.11.022

641 CHU, L., LIU, Q. sheng, HUANG, C., LIU, G. huan, 2016. Monitoring of winter wheat
642 distribution and phenological phases based on MODIS time-series: A case study in
643 the Yellow River Delta, China. J. Integr. Agric. 15, 2403–2416.
644 https://doi.org/10.1016/S2095-3119(15)61319-3

645 Cleland, E.E., Chuine, I., Menzel, A., Mooney, H.A., Schwartz, M.D., 2007. Shifting plant
646 phenology in response to global change. Trends Ecol. Evol. 22, 357–365.
647 https://doi.org/10.1016/J.TREE.2007.04.003

648 Dallimer, M., Tang, Z., Gaston, K.J., Davies, Z.G., 2016. The extent of shifts in vegetation
649 phenology between rural and urban areas within a human-dominated region. Ecol.
650 Evol. 6, 1942–1953. https://doi.org/10.1002/ece3.1990

651 Dong, Q., Chen, X., Chen, J., Zhang, C., Liu, L., Cao, X., Zang, Y., Zhu, X., Cui, X., 2020.
652 Mapping Winter Wheat in North China Using Sentinel 2A / B Data®: A Method
653 Based on Phenology-Time Weighted Dynamic Time Warping. Remote Sens.

654 ESA, 2015. SENTINEL-2 User Handbook 64. https://doi.org/GMES-S1OP-EOPG-TN-13-
655 0001

656 Garonna, I., De Jong, R., Stöckli, R., Schmid, B., Schenkel, D., Schimel, D., Schaepman,
657 M.E., 2018. Shifting relative importance of climatic constraints on land surface
658 phenology. Environ. Res. Lett. 13. https://doi.org/10.1088/1748-9326/aaa17b

659 Han, G., Xu, J., 2013. Land surface phenology and land surface temperature changes
660 along an urban-rural gradient in yangtze River Delta, China. Environ. Manage. 52,
661 234–249. https://doi.org/10.1007/s00267-013-0097-6

662 He, L., Asseng, S., Zhao, G., Wu, D., Yang, X., Zhuang, W., Jin, N., Yu, Q., 2015. Impacts
663 of recent climate warming, cultivar changes, and crop management on winter wheat
664 phenology across the Loess Plateau of China. Agric. For. Meteorol. 200, 135–143.
665 https://doi.org/10.1016/j.agrformet.2014.09.011

666 Huang, Y., Lu, L., 2009. Monitoring winter wheat phenology using time series of remote
667 sensing data. 2009 2nd Int. Conf. Inf. Comput. Sci. ICIC 2009 1, 135–138.

https://doi.org/10.1109/ICIC.2009.41

Imhoff, M.L., Zhang, P., Wolfe, R.E., Bounoua, L., 2010. Remote Sensing of Environment Remote sensing of the urban heat island effect across biomes in the continental USA. Remote Sens. Environ. 114, 504–513. https://doi.org/10.1016/j.rse.2009.10.008

Jochner, S., Menzel, A., 2015. Urban phenological studies - Past , present , future. Environ. Pollut. 203, 250–261. https://doi.org/10.1016/j.envpol.2015.01.003

Jochner, S.C., Sparks, T.H., Estrella, N., Menzel, A., 2012. The influence of altitude and urbanisation on trends and mean dates in phenology (1980–2009). Int. J. Biometeorol. 56, 387–394. https://doi.org/10.1007/s00484-011-0444-3

Kalnay, E., Cai, M., 2003. Impact of urbanization and land-use change on climate. Nature 423, 528–531. https://doi.org/10.1038/nature01675

Keenan, T.F., Gray, J., Friedl, M.A., Toomey, M., Bohrer, G., Hollinger, D.Y., Munger, J.W., O'Keefe, J., Schmid, H.P., Wing, I.S., Yang, B., Richardson, A.D., 2014. Net carbon uptake has increased through warming-induced changes in temperate forest phenology. Nat. Clim. Chang. 4, 598–604. https://doi.org/10.1038/nclimate2253

Lac, C., Donnelly, R.P., Masson, V., Pal, S., Riette, S., Donier, S., Queguiner, S., Tanguy, G., Ammoura, L., Xueref-Remy, and I., 2013. CO2 dispersion modelling over Paris region within the CO2-MEGAPARIS project. Atmos. Chem. Phys 4941–4961. https://doi.org/10.5194/acp-13-4941-2013

Land, D., Temperature, S., Azevedo, J.A., Chapman, L., Muller, C.L., 2016. Quantifying the Daytime and Night-Time Urban Heat Island in Birmingham , UK : A Comparison of Satellite Resolution Air Temperature Observations. https://doi.org/10.3390/rs8020153

Li, H., Zhou, Y., Li, X., Meng, L., Wang, X., Wu, S., Sodoudi, S., 2018. A new method to quantify surface urban heat island intensity. Sci. Total Environ. 624, 262–272. https://doi.org/10.1016/j.scitotenv.2017.11.360

Li, Xuecao, Zhou, Y., Asrar, G.R., Mao, J., Li, Xiaoma, Li, W., 2016. Response of vegetation phenology to urbanization in the conterminous United States. Glob. Chang. Biol. 23, 2818–2830. https://doi.org/10.1111/gcb.13562

Liu, S., Zhao, W., Shen, H., Zhang, L., 2016. Regional-scale winter wheat phenology monitoring using multisensor spatio-temporal fusion in a South Central China growing area. J. Appl. Remote Sens. 10, 046029. https://doi.org/10.1117/1.JRS.10.046029

Liu, Y., Chen, Q., Ge, Q., Dai, J., Qin, Y., Dai, L., Zou, X., Chen, J., 2018. Modelling the impacts of climate change and crop management on phenological trends of spring

and winter wheat in China. Agric. For. Meteorol. 248, 518–526. https://doi.org/10.1016/j.agrformet.2017.09.008

Louis, J., 2017. Sentinel-2 L2A Product Definition Document 1–36.

Lu, L., Wang, C., Guo, H., Li, Q., 2014. Detecting winter wheat phenology with SPOT-VEGETATION data in the North China Plain. Geocarto Int. 29, 244–255. https://doi.org/10.1080/10106049.2012.760004

Lu, P., Yu, Q., Liu, J., Lee, X., 2006. Advance of tree-flowering dates in response to urban climate change. Agric. For. Meteorol. https://doi.org/10.1016/j.agrformet.2006.04.002

Luo, Z., Sun, O.J., Ge, Q., Xu, W., Zheng, J., 2007. Phenological responses of plants to climate change in an urban environment. Ecol. Res. https://doi.org/10.1007/s11284-006-0044-6

Main-Knorn, M., Pflug, B., Debaecker, V., Louis, J., 2015. Calibration and validation plan for the l2A processor and products of the Sentinel-2 mission. Int. Arch. Photogramm. Remote Sens. Spat. Inf. Sci. - ISPRS Arch. 40, 1249–1255. https://doi.org/10.5194/isprsarchives-XL-7-W3-1249-2015

Manual, U., 2018. Sen2Cor Configuration and User Manual.

Meng, L., Mao, J., Zhou, Y., Richardson, A.D., Lee, X., Thornton, P.E., 2020. Urban warming advances spring phenology but reduces the response of phenology to temperature in the conterminous United States. Proc. Natl. Acad. Sci. U. S. A. 2–7. https://doi.org/10.1073/pnas.1911117117

Ou, J., Liu, X., Li, X., Li, M., Li, W., 2015. Evaluation of NPP-VIIRS nighttime light data for mapping global fossil fuel combustion CO2emissions: A comparison with DMSP-OLS nighttime light data. PLoS One 10. https://doi.org/10.1371/journal.pone.0138310

Parece, T., Campbell, J., 2018. Intra-Urban Microclimate Effects on Phenology. Urban Sci. 2, 26. https://doi.org/10.3390/urbansci2010026

Piao, S., Cui, M., Chen, A., Wang, X., Ciais, P., Liu, J., Tang, Y., 2011. Altitude and temperature dependence of change in the spring vegetation green-up date from 1982 to 2006 in the Qinghai-Xizang Plateau. Agric. For. Meteorol. 151, 1599–1608. https://doi.org/10.1016/j.agrformet.2011.06.016

Qiao, Z., Tian, G., Xiao, L., 2013. Diurnal and seasonal impacts of urbanization on the urban thermal environment: A case study of Beijing using MODIS data. ISPRS J. Photogramm. Remote Sens. 85, 93–101. https://doi.org/10.1016/j.isprsjprs.2013.08.010

Qiu, T., Song, C., Li, J., 2017. Impacts of urbanization on vegetation phenology over the past three decades in Shanghai, China. Remote Sens. 9, 1–16. https://doi.org/10.3390/rs9090970

738 Ren, G.Y., Zhou, Y.Q., Chu, Z.Y., Zhou, J.X., Zhang, A.Y., Gou, J., Liu, X.F., 2008.
739 Urbanization effects on observed surface air temperature trends in north China. J.
740 Clim. 21, 1333–1348. https://doi.org/10.1175/2007JCLI1348.1

741 Ren, Q., He, C., Huang, Q., Zhou, Y., 2018. Urbanization Impacts on Vegetation
742 Phenology in China. Remote Sens. 10, 1095. https://doi.org/10.3390/rs10121905

743 Samuel C Zipper and Jason Schatz et al., 2016. Urban heat island impacts on plant
744 phenology: intra-urban variability and response to land cover. Environ. Res. Lett. 11,
745 54023.

746 Schenker, G., Lenz, A., Körner, C., Hoch, G., 2014. Research paper Physiological
747 minimum temperatures for root growth in seven common European broad-leaved
748 tree species 302–313. https://doi.org/10.1093/treephys/tpu003

749 Shi, K., Huang, C., Yu, B., Yin, B., Huang, Y., Wu, J., 2014a. Evaluation of NPP-VIIRS
750 night-time light composite data for extracting built-up urban areas. Remote Sens.
751 Lett. 5, 358–366. https://doi.org/10.1080/2150704X.2014.905728

752 Shi, K., Yu, B., Huang, Y., Hu, Y., Yin, B., Chen, Z., Chen, L., Wu, J., 2014b. Evaluating the
753 ability of NPP-VIIRS nighttime light data to estimate the gross domestic product and
754 the electric power consumption of China at multiple scales: A comparison with
755 DMSP-OLS data. Remote Sens. 6, 1705–1724. https://doi.org/10.3390/rs6021705

756 Sisodia, P.S., Tiwari, V., Kumar, A., 2014. Analysis of Supervised Maximum Likelihood
757 Classification for remote sensing image. Int. Conf. Recent Adv. Innov. Eng. ICRAIE
758 2014 9–12. https://doi.org/10.1109/ICRAIE.2014.6909319

759 Sun, Y., Zhang, X., Ren, G., Zwiers, F.W., Hu, T., 2016. Contribution of urbanization to
760 warming in China. Nat. Clim. Chang. 6, 706–709.
761 https://doi.org/10.1038/nclimate2956

762 Tao, F., Yokozawa, M., Xu, Y., Hayashi, Y., Zhang, Z., 2006. Climate changes and trends
763 in phenology and yields of field crops in China, 1981-2000. Agric. For. Meteorol. 138,
764 82–92. https://doi.org/10.1159/000092636

765 Thebo, A.L., Drechsel, P., Lambin, E.F., 2014. Global assessment of urban and peri-urban
766 agriculture : irrigated and rainfed croplands. https://doi.org/10.1088/1748-
767 9326/9/11/114002

768 Wan, Z., 2014. New refinements and validation of the collection-6 MODIS land-surface
769 temperature/emissivity product. Remote Sens. Environ. 140, 36–45.
770 https://doi.org/10.1016/j.rse.2013.08.027

771 Wang, C., Chen, J., Wu, J., Tang, Y., Shi, P., Black, T.A., Zhu, K., 2017. A snow-free
772 vegetation index for improved monitoring of vegetation spring green-up date in

773 deciduous ecosystems. Remote Sens. Environ. 196, 1–12.
774 https://doi.org/10.1016/j.rse.2017.04.031

775 Wang, L., Chen, J., Gong, P., Shimazaki, H., Tamura, M., 2009. Land cover change
776 detection with a cross-correlogram spectral matching algorithm. Int. J. Remote Sens.
777 30, 3259–3273. https://doi.org/10.1080/01431160802562164

778 Wang, S., Ju, W., Peñuelas, J., Cescatti, A., Zhou, Y., Fu, Y., Huete, A., Liu, M., Zhang, Y.,
779 2019. Urban–rural gradients reveal joint control of elevated CO2 and temperature on
780 extended photosynthetic seasons. Nat. Ecol. Evol. 3. https://doi.org/10.1038/s41559-
781 019-0931-1

782 Wang, X., Gao, Q., Wang, C., Yu, M., 2017. Spatiotemporal patterns of vegetation
783 phenology change and relationships with climate in the two transects of East China.
784 Glob. Ecol. Conserv. 10, 206–219. https://doi.org/10.1016/j.gecco.2017.01.010

785 Wohlfahrt, G., Tomelleri, E., Hammerle, A., 2010. The urban imprint on plant phenology.
786 Nat. Ecol. Evol. https://doi.org/10.1038/s41559-019-1017-9

787 Xiao, D., Tao, F., Liu, Y., Shi, W., Wang, M., Liu, F., Zhang, S., Zhu, Z., 2013. Observed
788 changes in winter wheat phenology in the North China Plain for 1981-2009. Int. J.
789 Biometeorol. 57, 275–285. https://doi.org/10.1007/s00484-012-0552-8

790 Yan, G., Mas, J.F., Maathuis, B.H.P., Xiangmin, Z., Van Dijk, P.M., 2006. Comparison of
791 pixel-based and object-oriented image classification approaches - A case study in a
792 coal fire area, Wuda, Inner Mongolia, China. Int. J. Remote Sens. 27, 4039–4055.
793 https://doi.org/10.1080/01431160600702632

794 Yang, X., Ruby Leung, L., Zhao, N., Zhao, C., Qian, Y., Hu, K., Liu, X., Chen, B., 2017.
795 Contribution of urbanization to the increase of extreme heat events in an urban
796 agglomeration in east China. Geophys. Res. Lett. 44, 6940–6950.
797 https://doi.org/10.1002/2017GL074084

798 Yao, R., Wang, L., Huang, X., Guo, X., Niu, Z., Liu, H., 2017. Investigation of urbanization
799 effects on land surface phenology in Northeast China during 2001-2015. Remote Sens.
800 9, 1–17. https://doi.org/10.3390/rs9010066

801 Zhang, X., Friedl, M.A., Schaaf, C.B., Strahler, A.H., Schneider, A., 2004. The footprint of
802 urban climates on vegetation phenology. Geophys. Res. Lett. 31, 10–13.
803 https://doi.org/10.1029/2004GL020137

804 Zhang, X., Wang, J., Gao, F., Liu, Y., Schaaf, C., Friedl, M., Yu, Y., Jayavelu, S., Gray, J.,
805 Liu, L., Yan, D., Henebry, G.M., 2017. Exploration of scaling effects on coarse
806 resolution land surface phenology. Remote Sens. Environ. 190, 318–330.
807 https://doi.org/10.1016/j.rse.2017.01.001

Zhao, L., Lee, X., Smith, R.B., Oleson, K., 2014. Strong contributions of local background climate to urban heat islands. Nature 511, 216–219. https://doi.org/10.1038/nature13462

Zhou, D., Zhao, S., Zhang, L., Liu, S., 2016. Remotely sensed assessment of urbanization effects on vegetation phenology in China's 32 major cities. Remote Sens. Environ. 176, 272–281. https://doi.org/10.1016/j.rse.2016.02.010